Fully automated spatially resolved reflectance spectrometer for the determination of the absorption and scattering in turbid media

F. Foschum,[a] M. Jäger, and A. Kienle
Institut für Lasertechnologien in der Medizin und Meßtechnik an der Universität Ulm, Helmholtzstrasse 12, 89081 Ulm, Germany

(Received 28 June 2011; accepted 15 September 2011; published online 13 October 2011)

We describe a fully automated setup which is based on measurements of the spatially resolved reflectance for the determination of the reduced scattering and absorption coefficients in semi-infinite turbid media. The sample is illuminated with a xenon light source in combination with a monochromator enabling the scan of the wavelength from 450 nm to 950 nm. Reflected light from the sample is detected with a CCD camera providing a high spatial resolution. The essential steps for signal processing including, e.g., the consideration of the optical transfer function and the correct treatment of the background subtraction, are presented. The solutions of the diffusion theory and of the radiative transfer theory are investigated regarding the exact detection and illumination geometry. Systematic errors caused by using the different theories for fitting the optical parameters are characterized. The system was validated using liquid phantoms which contain Intralipid 20% and ink, and the measurement range of the system is specified. Further, we carefully characterized the optical properties of Intralipid 20% in the wavelength range between 450 nm and 950 nm. © *2011 American Institute of Physics*. [doi:10.1063/1.3648120]

I. INTRODUCTION

The light propagation in a turbid medium depends on its scattering and absorption properties. They can be determined noninvasively by measurement of the reflected light from the investigated sample, using different methods. Whereas it is not possible to distinguish between scattering and absorption from measurements of the total reflectance,[1,2] with methods such as the time resolved reflectance[3,4] and the frequency domain reflectance[5–7] one can determine the reduced scattering coefficient μ_s' and the absorption coefficient μ_a of a turbid medium. An alternative method is the measurement of the spatially resolved reflectance. Using this method the intensity of the reflected light from a sample is detected with respect to the distance to the illuminating spot. The measurement can be done either in contact with the sample using optical fibres[8–11] or in a non-contact procedure by imaging the intensity profile at the surface on a detector. There are mainly two methods for the non-contact procedure described in the literature. One is to image a small area of the surface to one detector and move this setup with respect to the source.[12–14] During this measurement the spectral information can be easily included using a spectrometer. The other technique which is the focus of this work is to image a larger section of the surface on a CCD detector. In the literature this setup is described by a couple of authors. Jacques *et al.*[15] presented a measurement system using a 8-bit camera. Because of the low dynamic range they had to capture several images with increasing integration time and piece the reflectance curve together. The CCD chip was thereby partly overexposed. Bolt *et al.*[16,17] used a 14-bit camera but they still had to piece the measurement together. Kienle *et al.*[18] used a 16- bit camera to record the measurement with a single image. With such a camera they could even see the influence of light scattered or reflected in the objective and tried to consider this by means of the point-spread function of the system.[19] In all these systems a laser is used for illumination, and therewith measurements at distinct wavelengths can be performed. All the authors, except Kienle *et al.*[18] used different solutions of the diffusion equation to determine the optical properties. Kienle *el al.*[18] solved the inverse problem using a neural network trained with Monte Carlo simulations which are solutions of the radiative transfer equation (RTE).

In this work, we present a fully automated spectroscopy system to determine the optical properties in the wavelength range from 450 nm to 950 nm. As we use a CCD based system, with which we can just measure with monochromatic light, a computer program written in DELPHI is used to scan through the wavelengths and to analyse the data. Thereby, the usable part of the reflectance curve is selected automatically by the program in order to avoid subjective evaluation of the results and to guarantee reproducible results. We improved the system by applying and comparing two methods to measure the optical transfer function of the system. The first method, introduced by Pilz *et al.*,[19] uses a delta source. The second one applies an extended source. Furthermore, we studied the time dependence of the background signal and present a solution to take this into account. In addition, the influence of the flat-field of the camera system is investigated. We also demonstrate a method to measure the scattered light at the illumination optics and examine its influence on the spatially resolved reflectance using Monte Carlo simulations. We describe a method to perform absolute measurements and compare absolute and relative measurements. For relative measurements an additional multiplicative factor is used in the theory.

[a]Electronic mail: florian.foschum@ilm.uni-ulm.de.

The solutions of the diffusion theory (DT) were compared with Monte Carlo simulations in which the whole setup geometry is regarded (MCd). We fitted reflectance curves calculated with DT to those computed by MCd and characterized the systematic errors due to the diffusion approximation. Furthermore, we applied a fitting routine using the standard Monte Carlo simulation (MCs) and investigated also the systematic errors.

Finally, measurements were performed on well characterized liquid phantoms using Intralipid 20% as scatterer[20] and ink as absorber to validate the experimental setup.

II. EXPERIMENT

The spatially resolved reflectance is measured with a 16-bit CCD camera (Pixis 512B, Princeton Instruments) having 512 × 512 pixels. To reduce noise the camera is cooled to nominal −70 °C by a multistage peltier element. We checked that the linearity of the chip is sufficient. An internal shutter guarantees that the CCD chip is illuminated during the exposure phase and not during the readout phase. For the measurement the surface of the illuminated sample is imaged in reduced size onto the CCD chip. To reduce the light scattered and reflected in the objective this is done by a single achromatic lens with anti-reflection coating for the visible spectral range ($f = 50$ mm, $d = 30$ mm, NT32-496, Edmund Optics). Using a single lens the magnification and the object plane are fixed. With the used optical system we image an approximately 50 mm × 50 mm section of the sample surface on the CCD chip. To further reduce the scattered light and to define the aperture diameter of the objective, three apertures are used as shown in Fig. 1. We applied a xenon lamp in combination with a monochromator as an illumination light source, see Fig. 2. This setup provides light from 450 nm to 950 nm with a minimum step size of 1 nm and a full width at half maximum of 15 nm. The almost unpolarized light is coupled into a ∅ = 400 μm optical fibre and can be switched on and off by a shutter. The sample-sided end of the optical fibre is imaged on the sample surface by an achromatic lens ($f = 80$ mm, $d = 25$ mm, Edmund Optics). The diameter of the spot at the surface is ∼500 μm, compare Sec. II D. An aperture behind the optical fibre avoids illumination of the lens mount. The optical path is folded by a mirror to decrease the illumination angle with respect to the surface normal. The

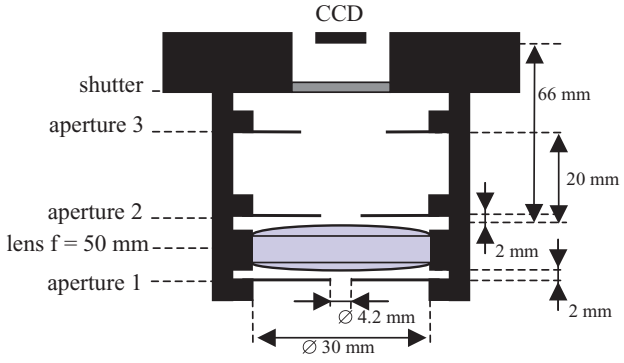

FIG. 1. (Color online) Detail of the objective used for the measurements.

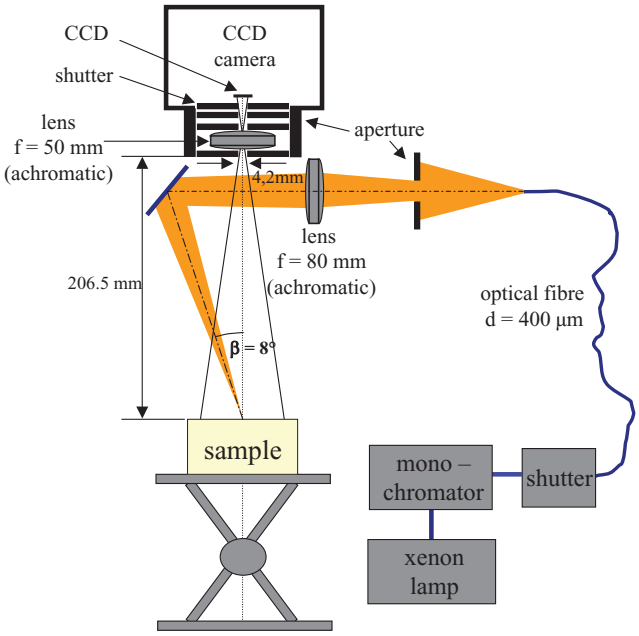

FIG. 2. (Color online) Schematic setup for spatially resolved reflectance measurements.

sample is illuminated with an angle of 8° with respect to the surface normal and, therewith, it is avoided that the specular reflex of a smooth surface hits the objective. When the surface is rough this is not the case anymore and the dynamic range remaining for the measurement of the reflectance from the sample bulk is reduced. The sample surface is adjusted to the object plane by the use of a height adjustable table. During the measurement procedure the following points have to be regarded. When an image of a sample is captured without illumination the camera detects a background signal of about 650 counts. This signal varies from pixel to pixel, over time and depends on the time since reading the last picture (compare Sec. II A). In addition, an equally bright surface in the object plane results in an inhomogeneous image on the CCD chip. This can be accounted for measurement of the systems flat-field (compare Sec. II B). Furthermore, scattered and reflected light and aberrations in the objective are the reasons why a point source in the object plane results in a non-point-like signal at the CCD. This effect can be considered by the optical transfer function (OTF) of the system (compare Sec. II C). In order to perform absolute measurements the power of the incident light and a calibration constant to convert pixel counts into power units have to be determined (compare Sec. II E). As the brightest point in the image of the turbid medium, illuminated at 8°, is not the center of the image (see Sec. II F), the center is determined with the method described in Sec. II F. For the conversion of pixel distances in the image into distances in the object plane the magnification has to be determined precisely. This is done by imaging a high contrast squared paper in the object plane to the CCD chip. Using a modified Hough transformation[21] the lines of the squared paper are found and described by analytical functions. The magnification is the result of the pixel distance between the lines at the CCD and the true distance of the lines

on the squared paper. Thereby, it is not necessary to align the lines along the pixels rows.

A. Background signal

The background values of the CCD camera pixels of a dark scene are not zero. This is caused, for example, by thermal effects on the CCD chip, readout noise, and residual light in the setup. The background has to be regarded by subtracting it from the illuminated picture. As the background changes slightly over time one way to estimate the background during the measurement is to measure it directly before and after the actual measurement and subtract the average of both. It turned out that the background is furthermore dependent on the time since the last picture has been taken. In Fig. 3 the mean value of all pixels of the background image is shown with respect to the time since the last picture was taken. For this study, a series of 20 images was captured, waiting for distinct times between the pictures. As shown in Fig. 3, the average background starts at ≈647 counts when images without delays are captured and converges to a value of ≈653 counts when we use a delay of 3000 ms or longer between the images. The difference of about six counts is not tolerable in the measurement. There are two ways to avoid this. First, one can wait for more than 3 s after each image so that the background has reached the final value. This would of course expand the measurement time. Second, the time between the pictures has to be kept constant. This was achieved in the following way. Before each measurement we captured a blanc image to clean the CCD chip. After 300 ms we captured the first background, then we again waited for 300 ms and captured the measurement. Finally, after another 300 ms we captured the second background. To perform this method it is necessary to have a computer controlled routine.

B. Flat-field

A spatial equal bright sample in the object plane does not result in equal pixel values over the whole CCD. This is caused, for example, by the different paths of the photons through the objective, dust on the CCD chip, or unequal sensitivity of each pixel. The flat-field is measured by using a scattering box, which is made of four white volume coloured plexiglass sheets (250 mm × 250 mm × 5 mm), mounted in parallel at a distance of 25 mm in a box. When this box is illuminated from below, the homogeneity of the intensity on the upper sheet was found to be sufficiently good. This was tested by moving the box laterally in the object plane and looking on just one pixel of the CCD chip. By masking the area outside the image area with a black cardboard the flat-field can be measured. The flat-field obtained for the introduced system shows deviations of about 5% in intensity. Applying this flat-field on measurements it turned out that there is only a small influence on the determination of the optical properties.

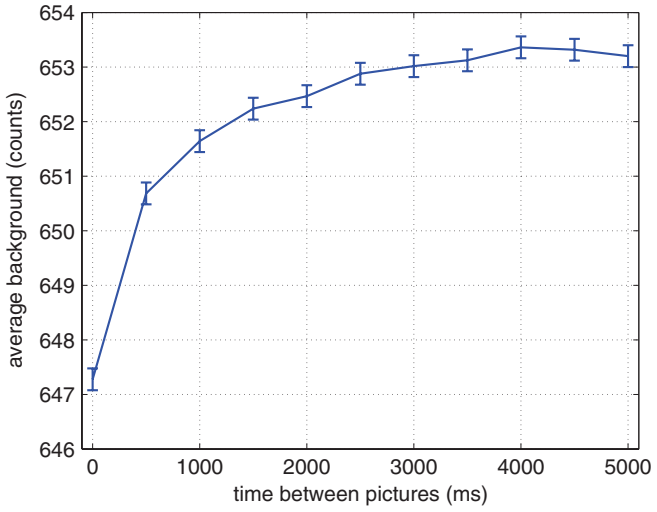

FIG. 3. (Color online) Dependence of the average background signal on the time passed since the last picture.

C. Optical transfer function

Imaging a delta point source in the object plane onto the CCD chip leads to signals at more than one pixel. The signal decreases with increasing distance to the center. This is caused mainly by aberrations of the lenses and light scattered or reflected in the objective. The effect can be described by the OTF of the system. Every illuminated point contributes according to this function to every other point. In the image we therefore get a convolution of the original signal with the OTF. The OTF was measured with two methods, namely, the delta source method (DSM) and the extended source method (ESM).

The DSM is already described in literature.[19,22] In this method, a monomode fibre is used as a delta source in the object plane, so that the OTF can be measured directly. Because the OTF degreases quite fast, with respect to the distance to the center, in a normal exposed image, the signal disappears after few pixels below the noise level. This image only holds information about the OTF for distances close to the source. But since the signal in the measurement is the convolution of the OTF and the real signal, also the values of the OTF at large distances are important. To measure these values the point source image can be overexposed by increasing the integration time by a factor of 100. In that way, the OTF signal for large distances is raised above the noise level. For this procedure an overexposure of the CCD chip causing blooming and other hardly predictable effects have to be accepted. Because of the blooming no values for short distances can be retrieved from this second image. The whole OTF can then be joint together from both measurements. The background has to be regarded as mentioned for the measurement on the scattering sample.

In addition, we developed an alternative method (ESM). Instead of a point source we use a homogeneously illuminated circular area in the object plane. As there is, integrated over the whole image, more light compared to the delta source image the signal is raised above the noise level for all distances. Therewith, we can retrieve the OTF with a single image. To create this circular area we use an integrating sphere (diameter 50 mm) with a sharp edged port of 5 mm diameter which is

aligned in the object plane facing the camera. The integrating sphere is illuminated from a side port with monochromatic light. The measured signal is now the convolution of the circular area and the OTF. For this measurement, one has to subtract the background as well. As the deconvolution of the measured signal with an ideal circular area leads to a quite noisy OTF, we instead convolve the theory. Based on the OTF measured with the DSM we estimated a parametrized analytical function for the OTF and determined the parameters by fitting the convolution of this OTF with an ideal circular area to the ESM measurement. The analytical function to describe the OTF is given by

$$T(\rho) = P_1 \exp(P_2\rho) + P_3 \exp(P_4\rho) + P_5 + P_6\rho, \qquad (1)$$

where P_1 to P_6 are the parameters to be fitted and ρ is the distance to the center. The convolution has to be done in (two-dimensional) 2D and is carried out using a 2D-FFT transformation. As the problem is radially symmetric, we calculate the average value for all pixels with the same distances to the center of the convolved theory and the measurement to fit the parameters. With these parameters the average error between the convolved theory and the measurement is smaller than 10%.

In Fig. 4 the OTFs determined at 530 nm with both methods are shown. As one can see, the two OTFs are similar, but the OTF measured with the ESM shows smaller values for large distances. Applying both OTFs on measurements one can observe that both OTFs lead to good results, but the OTF determined with the DSM overestimates the scattered light a little bit, whereas the OTF determined with the ESM underestimates it slightly. Consequently, we used the average of both methods. The parameters for the analytical OTF (Eq. (1)) obtained with the ESM are shown in Fig. 4.

The OTF changes within the wavelength. We measured the OTF of our system in the wavelength range from 450 nm to 950 nm in steps of 20 nm with both methods. We observed that the values of the OTF at large distances decrease from 450 nm to 550 nm and rise again for wavelengths up to 950 nm. The difference between the lowest and the highest value is larger than one order of magnitude. This means that if we scan through the wavelength with the system we have to regard a wavelength dependent OTF. We found that the step size of 20 nm is sufficient. When we measure at a distinct wavelength, we use the OTF measured at the closest wavelength.

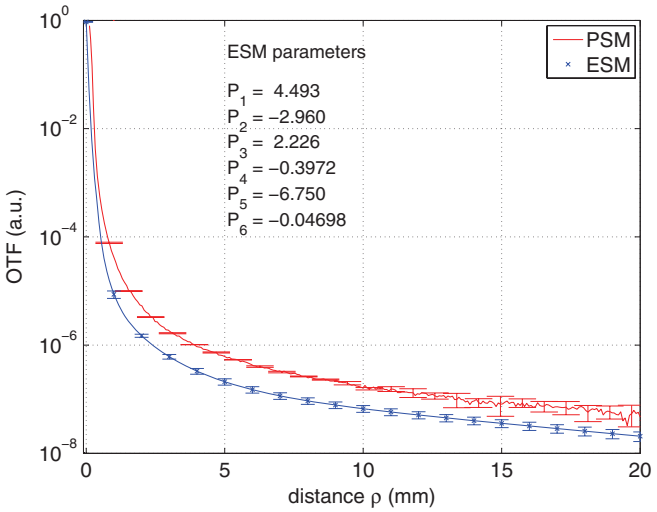

FIG. 4. (Color online) Comparison of the OTF determined with the DSM and ESM.

There are two ways to apply the OTF to the measurements. One can convolve the theory with the OTF. As every point in the theory contributes to every point in the convolved signal this can only be done when the theory represents the measurement in all points. By using the DT this is not valid, because the lower values at short distances in the DT compared to MC (see Sec. III C) lead to wrong contributions in the other distances. The other method is to deconvolve the measurement signal with the OTF. By applying the used analytical function, we checked that the deconvolution is valid. In this work, we use the deconvolution process noticing that the noise is increased by this procedure.

D. Illumination beam profile

The illumination beam profile can be measured with the setup itself. We used a rough aluminium plate in the object plane assuming that the angular reflectance is constant within the used small angular range. The penetration depth of the light in the aluminium is negligible. By measuring with an optimal integration time the main peak is well imaged, but the intensity for large distances is lower than the noise level. To measure these values we drilled a $\oslash = 4$ mm hole in aluminium and performed a second measurement with 100 times higher integration time by shining the beam center through the hole. Therewith, we avoid the overexposure of the chip in the main spot. The beam profile can then be determined by combining the measurement with normal exposure for distances up to 2 mm with the overexposed measurement for distances larger than 2 mm. The overexposed measurement has to be divided by the factor of 100. The radially averaged beam profile of our system is shown in Fig. 5. In this profile, the intensity drops down to almost 1/e compared to the intensity in the center at a radius of 250 μm. The scattered light by the illumination optics at the object plane can be clearly observed, see Fig. 5. Even at large distances ($\approx$20 mm) this causes a contribution which is approximately seven orders of magnitude of the intensity at the center. We found that the beam profile does not significantly depend on the wavelength and, therefore, we used the profile measured at 550 nm for the MCd.

E. Absolute measurements

To get absolute values from the CCD image the incident power P_M on the sample and a calibration constant to convert pixel values into power units have to be determined. The incident power was measured with an optical powermeter (Optometer S370, UDT). The calibration constant was determined with the following procedure. A monochromatic, collimated light beam with a diameter less than the aperture of the

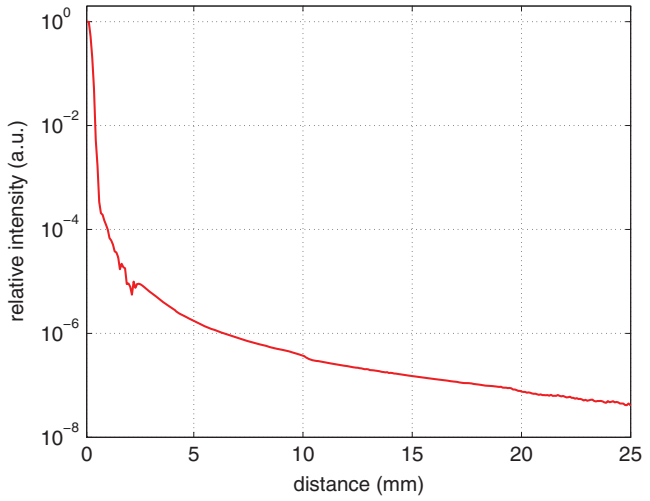

FIG. 5. (Color online) Beam profile of the introduced system measured at 550 nm.

objective is imaged on the CCD chip and the sum of the count values from all illuminated pixels C_{cal} is calculated. Using the powermeter the power P_{cal} of the collimated light beam can be measured. The calibration factor is expressed by

$$F_{cal} = \frac{P_{cal} t_{cal}}{C_{cal} A_{\text{Pixel}}} \left[\frac{\text{Ws}}{\text{count mm}^2} \right], \tag{2}$$

where the integration time t_{cal} has to be regarded as it differs from that in the measurement. The area of one pixel A_{Pixel} has also to be considered. Within the measurement the absolute reflectance R can be calculated for each pixel from its value C_M by

$$R = \frac{C_M F_{cal}}{t_M P_M} K_{fres} [\text{mm}^{-2}] \tag{3}$$

by taking the integration time of the measurement t_M into account. If not already regarded in the theory one has to consider the reflections at the boundary by the mean Fresnel coefficient K_{fres}. The collimated light beam was produced by means of a 50 μm optical fibre in the focus of a $f = 40$ mm lens. The diameter of the beam was selected by a tunable aperture right behind the lens. By fitting the measurement, we found that for the used optical properties absolute measurements are not necessary to obtain good results. Therefore, in this paper we did not perform absolute measurements. However, for higher reduced scattering and absorption coefficients they have advantages compared to relative measurements.

F. Determination of the center of the image

In order to find the center of the rotational symmetric image at large distances, we used the following procedure. This is necessary because in scattering media the incident point moves slightly lateral in the object plane due to the non-perpendicular incidence and the brightest point is not the center. Therefore, we look for all pixels in the measurement image which show pixel values of 0.1% ± 10% compared to the brightest pixel in the image. As in samples with isotropic light propagation these pixels are positioned on a circle around the center, we calculate its coordinates by fitting a circle function. The fit parameters are hereby the coordinates of the center and the radius of the circle. Extracting the center from the measurement image makes the method more robust.

G. Measurement procedure

To conclude the measurement procedure a flow chart of the computer program is shown in Fig. 6. First, the optimal integration time which leads to a maximum pixel value of 50 000 counts is determined for the selected wavelength and sample. Therefore, an image with low integration time is captured and, based on a linear behaviour between integration time and pixel values, the optimal integration time is calculated. With this integration time the measurement is collected as mentioned in Sec. II A as a series of dark and illuminated images and under subtraction of the background measurement. To reduce noise this procedure is repeated five times and the average of all measurements is calculated. For samples with rough surfaces, for which the dynamic range is reduced because of the surface reflections more repetitions can be necessary. The averaged image is then corrected by the flat-field of the system and deconvolved by the OTF. Once the image center is determined, all pixels with the same distance to the center are averaged. The result is the reflectance versus the distance to the light source which is used for the determination of the optical properties.

Before the optical coefficients can be determined with the nonlinear regression the evaluable part of the curve has

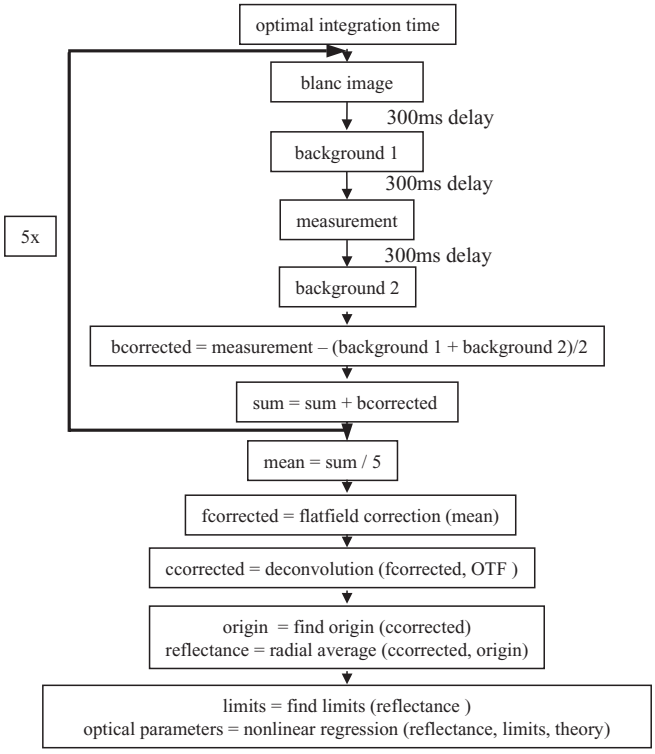

FIG. 6. Scheme of the measurement procedure.

to be selected. The short distances of the reflectance curve have to be ignored to improve the results, because there the influence of the setup geometry, of the phase function of the turbid medium and of the diffusion approximation (see Sec. III A) is large. The optimal start distance depends on the optical properties. In this work, we evaluated the reflectance curve from distances starting at $\rho = 1/\mu_s'$. As the reduced scattering coefficient is unknown in advance its value was estimated by multiple fitting of the data using the start distance according to the μ_s' in the last iteration. The maximum distance is limited by the magnification of the system. In the case of our setup, we can, in principle, measure up to 23 mm. In highly scattering and absorbing media the reflectance decreases fast with increasing distance. Therefore, the signal falls beyond the noise level after distances smaller than 23 mm. By use of the 16-bit camera, approximately four orders of magnitudes can be resolved. Due to dynamic range reduction caused by surface reflections and noise, effectively three orders of magnitudes can be used for fitting when distances smaller than $1/\mu_s'$ are ignored. Thus, the distance up to which the measurement is evaluated is either 23 mm or the distance where the signal decreases three orders of magnitudes with respect to the start distance at $1/\mu_s'$. Finally, the optical coefficients are determined by nonlinear regression using theoretical reflectance curves.

III. THEORY

There are usually two ways to calculate theoretical reflectance curves from turbid media. For a semi-infinite medium the reflectance can be expressed by an analytical function based on the diffusion approximation. A more exact solution however can be found within RTE. As there is, according to the author's knowledge, no useful analytical solution for the semi-infinite reflectance of the RTE the solution has to be calculated numerically, e.g., by means of Monte Carlo simulations. In this simulation arbitrary setup geometries can be regarded.

A. Diffusion theory

There are different methods to derive the reflectance from a semi-infinite medium within the DT. We used the expression described by Kienle *et al.*[23] which uses extrapolated boundary conditions. The reflectance is described by one term proportional to the fluence and another proportional to the flux. The Fresnel coefficients needed for this boundary conditions can be calculated according to Haskell *et al.*[24] The diffusion approximation predicts the reflectance well, if the distance to the source is large and the absorption coefficient is much smaller than the reduced scattering coefficient. In this work, the diffusion constant $D = \frac{1}{\sqrt{3(\mu_a+\mu_s')}}$ is used.

B. Monte Carlo method

To solve the radiative transfer equation we used our Monte Carlo code, whose principles are similar to those described by Wang *et al.*[25] The simulation traces single "photons" through the medium. In the standard case (MCs), all photons which leave the medium in a distinct area are collected for the reflectance and the absolute value, measured by a detector of finite aperture, are calculated using an angular cosine dependence of the reflected photons. For this simulation, we illuminate the sample perpendicularly to the surface with a point source. For the standard case the calculation can be accelerated by application of the single Monte Carlo method[26] which we extended for the spatially resolved steady state case (single MCs).

For the second MC simulation the detector geometry of our measurement setup (MCd) was considered. The measured illumination profile and the incident angle of 8° were included. Also, the two-dimensional discretisation of the signal as caused by using a CCD and the determination of the image center (see Sec. II F) were considered. Another point is the finite aperture of the objective. As investigated in an earlier work,[27] the angular distribution of the exiting photons from a semi-infinite medium follows, in general, not a cosine dependence. Especially, for small distances to the source this causes differences in the reflectance compared to the MCs. When we include a detector with an aperture, as used in the measurement, and just collect the photons passing it, the calculation time is significantly increased. Therefore, we added a variance reduction method for small detectors introduced by Poole *et al.*[28] to the Monte Carlo code and extended it by the refraction at the surface. At every interaction point in the medium the probability of the photon to hit the detector within the next step is calculated using this method. For the extension to the nonmatched conditions the point where the photon leaves the medium was calculated using Fermat's law and Fresnel reflection coefficients were considered. For the MCd the single Monte Carlo method cannot be applied because the angular distribution is not scalable.

C. Comparison of the methods

In this section, the reflectance calculated by the DT, MCs, and MCd is compared. For the simulations a reduced scattering coefficient of $\mu_s' = 1.0\ \text{mm}^{-1}$, a refractive index of $n = 1.33$, an anisotropy factor of $g = 0.75$ in combination with the Henyey-Greenstein phase function, and two different absorptions coefficients ($\mu_a = 0.001\ \text{mm}^{-1}$ and $\mu_a = 0.1\ \text{mm}^{-1}$) were assumed. The reflectances calculated with 10^7 photons for the MCd and MCs are shown in Fig. 7. In addition, the calculations of the reflectance using the DT is given in the figure. The comparison of both Monte Carlo simulations shows that for short distances ($\rho < 1$ mm) the beam profile, which is only considered in the MCd, affects the reflectance. For distances larger than 1 mm the reflectance shows almost the same shape, but the reflectance simulated with the MCd is up to 10% higher than the reflectance calculated with MCs. It can be figured out that this is caused by the angular distribution of the remitted photons which differ from the cosine dependence. Especially, for absolute measurements this effect has to be regarded.

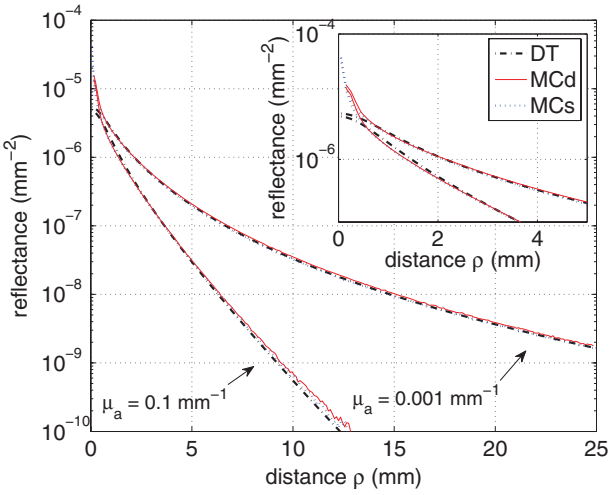

FIG. 7. (Color online) Comparison of the MCd, MCs, and DT for different absorption coefficients.

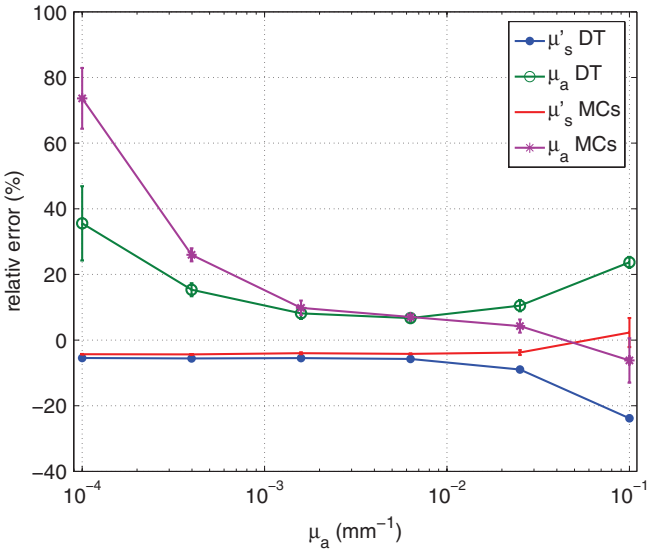

FIG. 8. (Color online) Relative errors of the optical parameters obtained by fitting the reflectance calculated with MCd using the solutions of DT and MCs.

Considering the DT, it can be shown that for small distances there is a disagreement between the DT and the MCs. The DT curve starts with much lower reflectance values for short distances, rises for middle distances (0.5 mm to 2 mm) above the MCs reflectance and converges to the MCs for large distances. The low values at the start distance are caused, e.g., by using a single point source in the DT. This can be improved by applying an exponentially decreasing source, but as this would just influence the small distances which are excluded in the evaluation of the measurement there is no improvement for the determination of the optical properties. The higher values at distances between 0.5 mm $<\rho <$ 2 mm are caused by the approximations in the DT and get worse when the absorption coefficient is increased. Also, there is no good agreement between DT and MCs for high μ_a. For low absorption, however, the DT describes the reflectance calculated with MCs simulations well.

D. Fitting procedure

We retrieve the optical coefficients by means of a nonlinear regression. For the fit the theoretical reflectance curves are calculated by the DT and single MCs simulations. For the nonlinear regression the Levenberg-Marquardt algorithm is used. It turned out, that better results for the optical properties can be obtained when the logarithm of the reflectance is fitted with constant weights for all values. Therewith, the reflectance at large distances is weighted more than if linear reflectance curves are fitted using the weights calculated with the standard deviation. The absolute fit has some disadvantages and therefore, we just perform relative fits. For relative measurements an additional multiplicative factor is used in the theory. The disadvantages are that the conversion to absolute values is complicated and time consuming, the uncertainties of the assumed parameters (refractive index and phase function) have a larger influence and there is often no improvement in the accuracy in the determination of the optical properties.

E. Errors caused by fitting with DT and MCs

To estimate the systematic errors caused by using the DT or MCs to fit the optical parameters a series of MCd simulations were calculated. From this reflectance curves the optical parameters were obtained by fitting with DT and the single MCs method. The relative errors compared to the parameters in the MCd simulations were calculated and are shown in Fig. 8. The parameters in the MCd simulations were $\mu_s' = 1.0$ mm^{-1}, $n_M = 1.33$, and $g = 0.75$ (Henyey-Greenstein function) and the absorptions coefficient was varied in the range of 0.0001 mm^{-1} $< \mu_a <$ 0.1 mm^{-1}. Concerning the determination of the reduced scattering coefficient both methods are comparable. Using the DT, we get a systematic error in μ_s' of about 6% for a large range of absorption coefficients. For large μ_a the diffusion theory starts to break down and the results get worse. In this region the MCs can improve the results which causes an error of ~5%. In the determination of μ_a both theories are comparable. The errors for typically used absorption coefficients are smaller than 10% but they can increase up to 40% for very low and very high absorption coefficients. For large μ_a the MCs are slightly better than the DT, but for small μ_a this theory causes larger errors. Altogether, there is no big advantage in using the MCs instead of the DT because both do not consider the real illumination and detection geometry and the single MCs are more time consuming. For the evaluation of the measurements of samples the DT was used exclusively.

F. Errors due to wrong assumptions of the phase function and the refractive index

When measurements on, for example, biological tissues are performed, often the refractive index and the phase function of the turbid medium are not known. To quantify the errors in the determination of the optical properties assuming an incorrect value of these coefficients, MCs simulations are

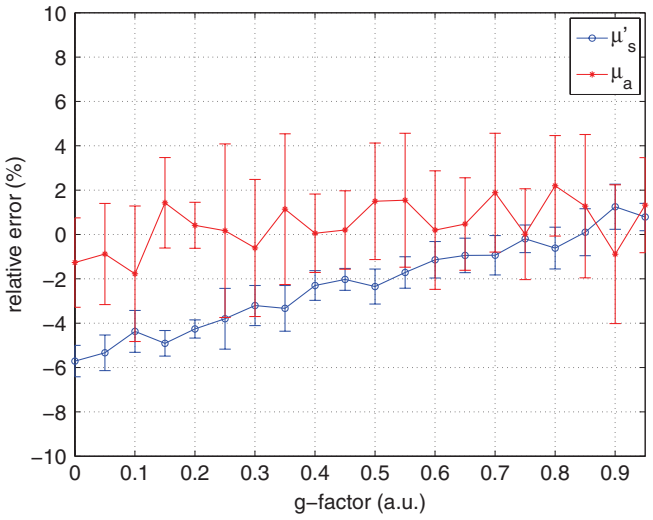

FIG. 9. (Color online) Errors in the optical coefficients assuming a wrong g-factor (Henyey-Greenstein function).

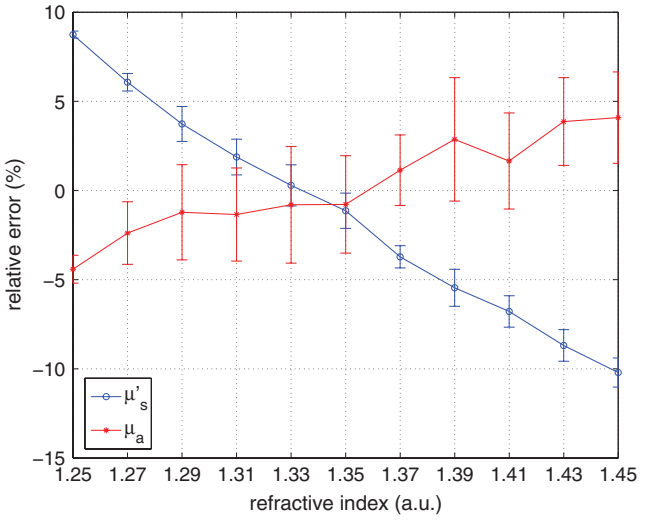

FIG. 10. (Color online) Errors of the optical coefficients assuming a wrong refractive index.

calculated and fitted with MCs simulation with the wrong assumptions of these coefficients. For the first study a set of MCs simulations with $\mu_s' = 1.0$ mm^{-1}, $\mu_a = 0.01$ mm^{-1}, $n_M = 1.33$ was calculated. The g-factor was varied from $g = 0$ to $g = 0.95$ (Henyey-Greenstein function). The relative errors of μ_a and μ_s' obtained by fitting these curves with MCs (relative fit) assuming $g = 0.75$ (Henyey-Greenstein function) are shown in Fig. 9. There is almost no influence on the determination of μ_a. The determination of μ_s' is influenced most if the g-factor is low, where errors up to 5% can occur. Therewith, the g-factor has only a small influence on the determination of the optical properties for not too small g.

In a further study, the phase function was changed to a more realistic one. First, the measured phase function for Intralipid 20% (Ref. 29) and second the phase function for TiO_2 spheres (diameter $= 7$ μm) in epoxy resin ($n_s = 2.7$, $n_m = 1.57$) calculated with Mie theory were used. The MCs simulations using these phase functions were fitted using the MCs simulations with the same g-factor and the Henyey-Greenstein phase function. The resulting errors in μ_s' were 3% and 7%, respectively. The errors in μ_a were 5% and 10%, respectively, for standard parameters.

Furthermore, the influence of uncertainties in the refractive index of the medium was investigated. Therefore, the refractive index was varied from $n = 1.25$ to $n = 1.45$ in the same procedure as described above. The errors resulting from the fit are shown in Fig. 10. The influence on the determination of the absorption coefficient is smaller than 5%. If the refractive index is assumed too small then also the absorption coefficient is determined too small and vice versa. The reduced scattering coefficient is affected more by the wrong assumption of the refractive index. There is an error of $\sim$10% for a change of 0.1 in the refractive index. Contrarily to the absorption coefficient the reduced scattering coefficient is determined too large when the refractive index is underestimated. We point out, that these errors increase when absolute measurements are performed.

IV. MEASUREMENTS ON PHANTOM MEDIA

For testing the setup, liquid phantoms were made from Intralipid 20% (Fresenius Kabi, Bad Homburg, Germany) and black ink (Pelikan, Hannover, Germany). In contrast to Indian ink (suspended carbon particles), the used ink is a solution of different dyes. As it is therewith a molecular absorber with negligible scattering, one can measure its absorption coefficient with a spectrophotometer. To avoid a spectral shift of the absorption band caused by pH changes we used a buffer solution of pH $= 8.0$ (Merck, Darmstadt, Germany) as a diluting agent to stabilize the pH in the phantoms. By changing the concentration of ink and Intralipid we can test the measurement system and are able to investigate the measurement range. For this study, three phantoms with Intralipid 20% and a buffer solution with concentrations of $C_L = 0.0376$ ml/ml, $C_L = 0.0574$ ml/ml, and $C_L = 0.0734$ ml/ml (V1 - V3) without ink were produced. The reduced scattering coefficient was, thus, between 0.7 mm^{-1} and 2.8 mm^{-1}. In addition, two phantoms with Intralipid, ink, and a buffer solution were mixed, having both a concentration of Intralipid of $C_L = 0.046$ ml/ml and a concentration of ink of $C_I = 2.77910^{-5}$ ml/ml (V4) and $C_I = 2.51410^{-4}$ ml/ml (V5), respectively. All five phantoms were measured with the introduced procedure from 450 nm to 950 nm with a step size of 20 nm. The optical properties were determined by fitting the measured reflectance with the solution of the DT. The wavelength dependent refractive index of water was used as a refractive index for the medium.

In Fig. 11 the reflectance curves at distinct wavelengths for the phantom V4 before and after the corrections(see Sec. II) are shown. It can be seen that the corrections are essential to determine the right optical properties. Even for the reflectance curve which decreases slowly with increasing distance the correction changes the signal.

The result of the reduced scattering coefficient of the pure Intralipid 20%, calculated by considering the concentration, measured on the five phantoms is shown in Fig. 12. The wavelength dependence of the reduced scattering coefficient can

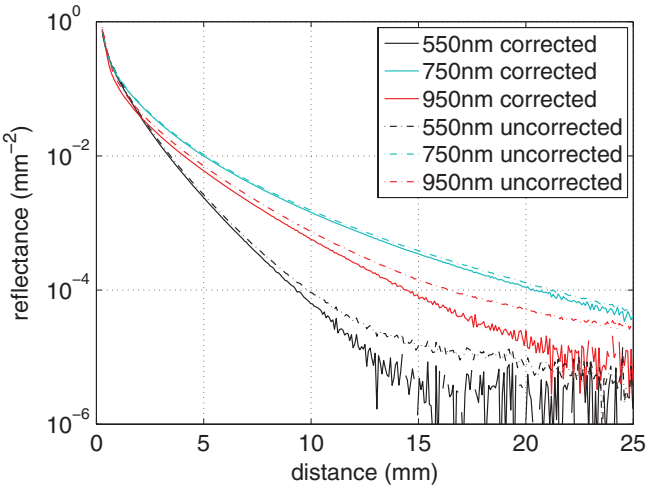

FIG. 11. (Color online) Spatially resolved reflectance curves measured from an Intralipid 20% phantom (V4). The raw data and the corrected reflectance are shown.

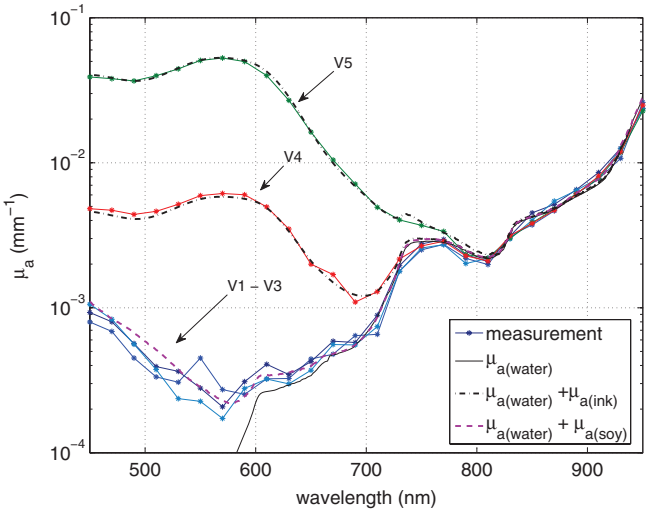

FIG. 13. (Color online) Absorption coefficient of the five different phantoms next to the expected absorption as a combination of water absorption, soy oil absorption, and ink absorption under consideration of the concentration.

be described by the power law $\mu_s' = a\lambda^{-b}$. The coefficients obtained with the power law are also shown in Fig. 12. The results for the different phantoms agree within less than 3%. Considering the systematic errors caused by using the DT the reduced scattering coefficient can be determined with an error smaller than ~6%. Even for the high concentration of the ink in the phantom no crosstalk on the reduced scattering coefficient can be observed.

In Fig. 13 the corresponding absorption coefficient of the phantoms is shown. The absorption coefficient can be compared with the water absorption[30,31] and the ink absorption measured with a spectrophotometer (Cary 5000, Varian). The absorption curves considering the concentration of the ink are also shown. The absorption of the phantoms without ink follows nicely the water absorption for wavelengths larger than 600 nm. For wavelengths below 600 nm the absorption coefficient is higher than the water absorption. This is caused by the soy oil in the Intralipid 20%. The soy oil absorption was measured by destroying the lipid vesicles[32] of the Intralipid using isopropyl alcohol and extracting the oil. The expected absorption of the Intralipid dilution V2 consisting of water and soy oil absorption is plotted in Fig. 13 showing a good agreement with the results of the spatially resolved reflectance measurements. When ink is added, the absorption rises mainly in the region between 450 nm and 750 nm. Thereby, the measured absorption with the spatially resolved reflectance follows the predicted values. The errors between the measured and the predicted absorption coefficient are smaller than 20%.

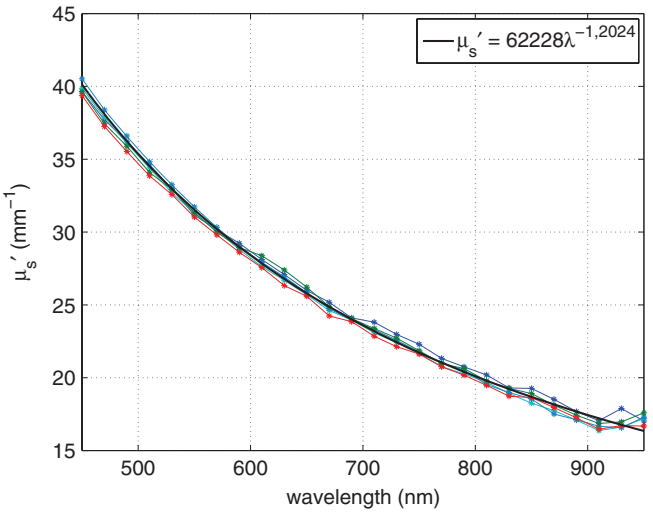

FIG. 12. (Color online) Reduced scattering coefficients for the pure Intralipid 20% of the five different phantoms.

Due to further measurements in which the absorption and the reduced scattering coefficients were varied the measurement range of the system could be determined. We found our system to work within the given accuracy when the reduced scattering coefficient is in the range of 0.8 mm^{-1} $< \mu_s'$ $<$ 8 mm^{-1} and the absorption coefficient is in the range of 0.0001 mm^{-1} $< \mu_a <$ 0.02 mm^{-1}.

In biological tissue at short wavelengths the absorption coefficient is often higher than 0.02 mm^{-1}. To measure these values, we can use *a priori* information of the reduced scattering coefficient. In most tissues there are spectral regions where the absorption is low and the reduced scattering coefficient can be determined. Furthermore, μ_s' can be described by the power law in many turbid media. By fitting the power law in the spectral region where we can measure μ_s' it can be extrapolated to the lower wavelengths with good accuracy. When this μ_s' is assumed at these wavelengths and just μ_a and the multiplicative constant are fitted we can determine μ_a even for higher values.

V. CONCLUSION

In summary, we presented a fully automated setup for determination of the optical properties in a turbid media based on measurements of the spatially resolved reflectance using a CCD camera. We introduced the essential steps which have to be considered for performing the measurements. We pointed

out that it is very important to consider the optical transfer function and the dependence of the background on the time passed since the last picture. As for the theory, exact simulations regarding the setup geometry were performed and it was found that the diffusion theory is valid for determination of the optical properties in the indicated range. The systematic errors caused by using the diffusion theory were estimated for our system. The errors are mainly caused by the geometry of the measurement system. In addition, we measured liquid Intralipid 20% phantoms confirming that the optical properties can be determined with errors in μ_s' and μ_a below 6% and below 20%, respectively. Further, we carefully characterized the absorption of Intralipid 20% in the wavelength range between 450 nm and 950 nm, obtaining good results even between 450 nm and 700 nm, where the absorption is low.

In further work, we will focus to extend our system for measurements on media with higher absorption coefficients. Therefore, a fitting routine using MCd as a forward model will be applied. We will also train a neural network to determine the optical properties using MCd. Applying a neural network the optical properties of a turbid medium can be determined in less than one second for the whole spectral range.

ACKNOWLEDGMENTS

We acknowledge the financial support by the Deutsche Forschungsgemeinschaft (DFG).

[1]B. Wilson and S. Jacques, IEEE J. Quantum Electron. **26**, 2186 (1990).
[2]S. Flock, S. Jacques, B. Wilson, W. Star, and M. van Gemert, Lasers Surg. Med. **12**, 510 (1992).
[3]M. Patterson, B. Chance, and B. Wilson, Appl. Opt. **28**, 2331 (1989).
[4]A. Pifferi, A. Torricelli, P. Taroni, D. Comelli, A. Bassi, and R. Cubeddu, Rev. Sci. Instrum. **78**, 053103 (2007).
[5]M. Patterson, J. Moulton, B. Wilson, K. Berndt, and J. Lakowicz, Appl. Opt. **30**, 4474 (1991).
[6]B. Tromberg, O. Coquoz, J. Fishkin, T. Pham, E. Anderson, J. Butler, M. Cahn, J. Gross, V. Venugopalan, and D. Pham, Philos. Trans. R. Soc. London **352**, 661 (1997).
[7]J. Fishkin, O. Coquoz, E. Anderson, M. Brenner, and B. Tromberg, Appl. Opt. **36**, 10 (1997).
[8]M. Patterson, E. Schwartz, and B. Wilson, Proc. SPIE **1065**, 115–122 (1989).
[9]B. Wilson, M. Patterson, and B. Pogue, Proc. SPIE **1892**, 132–147 (1993).
[10]M. Nichols, E. Hull, and T. Foster, Appl. Opt. **36**, 93 (1997).
[11]R. Doornbos, R. Lang, M. Aalders, F. Cross, and H. Sterenborg, Phys. Med. Biol. **44**, 967 (1999).
[12]R. Groenhuis, H. Ferwerda, and J. Bosch, Appl. Opt. **22**, 2456 (1983).
[13]R. Groenhuis, J. Bosch, and H. Ferwerda, Appl. Opt. **22**, 2463 (1983).
[14]S. Andree, C. Reble, J. Helfmann, I. Gersonde, and G. Illing, J. Biomed. Opt. **15**, 067009 (2010).
[15]S. Jacques, A. Gutsche, J. Schwartz, L. Wang, and F. Tittel, Medical Optical Tomography: Functional Imaging and Monitoring **11**, 211–226 (1993).
[16]R. Bolt and J. Ten Bosch, Appl. Opt. **32**, 4641 (1993).
[17]R. Bolt and J. Bosch, Waves in Random Complex Media **4**, 233 (1994).
[18]A. Kienle, L. Lilge, M. Patterson, R. Hibst, R. Steiner, and B. Wilson, Appl. Opt. **35**, 2304 (1996).
[19]M. Pilz, S. Honold, and A. Kienle, J. Biomed. Opt. **13**, 054047 (2008).
[20]F. Martelli and G. Zaccanti, Opt. Express **15**, 486 (2007).
[21]R. Duda and P. Hart, Commun. ACM **15**, 11 (1972).
[22]H. Du and K. Voss, Appl. Opt. **43**, 665 (2004).
[23]A. Kienle and M. Patterson, J. Opt. Soc. Am. A **14**, 246 (1997).
[24]R. Haskell, L. Svaasand, T. Tsay, T. Feng, M. McAdams, and B. Tromberg, J. Opt. Soc. Am. A **11**, 2727 (1994).
[25]L. Wang, S. Jacques, and L. Zheng, Comput. Methods Programs Biomed. **47**, 131 (1995).
[26]A. Kienle and M. Patterson, Phys. Med. Biol. **41**, 2221 (1996).
[27]A. Kienle and F. Foschum, Opt. Express **19**, 3881 (2011).
[28]L. Poole, D. Venable, and J. Campbell, App. Opt. **20**, 3653 (1981).
[29]R. Michels, F. Foschum, and A. Kienle, Opt. Express **16**, 5907 (2008).
[30]L. Kou, D. Labrie, and P. Chylek, Appl. Opt. **32**, 3531 (1993).
[31]R. Pope and E. Fry, Appl. Opt. **36**, 8710 (1997).
[32]H. Van Staveren, C. Moes, J. van Marie, S. Prahl, and M. van Gemert, Appl. Opt. **30**, 4507 (1991).